Available online at www.sciencedirect.com
ScienceDirect
Magnetic Resonance Imaging 28 (2010) 1258–1269
MAGNETIC RESONANCE IMAGING

Retinotopic mapping with spin echo BOLD at 7T

Cheryl A. Olman[a,b,*], Pierre-Francois Van de Moortele[b], Jennifer F. Schumacher[c], Joseph R. Guy[a], Kâmil Uğurbil[b], Essa Yacoub[b]

[a]Department of Psychology, University of Minnesota, Minneapolis, MN 55455, USA
[b]Department of Radiology, University of Minnesota, Minneapolis, MN 55455, USA
[c]Graduate Program in Neuroscience, University of Minnesota, Minneapolis, MN 55455, USA

Received 6 January 2010; revised 17 March 2010; accepted 10 June 2010

Abstract

For blood oxygenation level-dependent (BOLD) functional MRI experiments, contrast-to-noise ratio (CNR) increases with increasing field strength for both gradient echo (GE) and spin echo (SE) BOLD techniques. However, susceptibility artifacts and nonuniform coil sensitivity profiles complicate large field-of-view fMRI experiments (e.g., experiments covering multiple visual areas instead of focusing on a single cortical region). Here, we use SE BOLD to acquire retinotopic mapping data in early visual areas, testing the feasibility of SE BOLD experiments spanning multiple cortical areas at 7T. We also use a recently developed method for normalizing signal intensity in T_1-weighted anatomical images to enable automated segmentation of the cortical gray matter for scans acquired at 7T with either surface or volume coils. We find that the CNR of the 7T GE data (average single-voxel, single-scan stimulus coherence: 0.41) is almost twice that of the 3T GE BOLD data (average coherence: 0.25), with the CNR of the SE BOLD data (average coherence: 0.23) comparable to that of the 3T GE data. Repeated measurements in individual subjects find that maps acquired with 1.8-mm resolution at 3T and 7T with GE BOLD and at 7T with SE BOLD show no systematic differences in either the area or the boundary locations for V1, V2 and V3, demonstrating the feasibility of high-resolution SE BOLD experiments with good sensitivity throughout multiple visual areas.

Keywords: Functional magnetic resonance imaging; Retinotopic mapping; Visual cortex; Brain mapping/methods; Humans

1. Introduction

As neuroscientists look for more information about how the spatial distribution of activity within different cortical areas encodes information, it is increasingly valuable to take advantage of very high magnetic fields to use fMRI to map neural responses with improved precision. The advantages of ultra-high-field fMRI have been well described [1–3]. These include an improved signal-to-noise ratio (SNR) that enables higher resolution [4], amplified blood oxygenation level-dependent (BOLD) effects in gray matter that improve the contrast-to-noise ratio (CNR) and a short venous blood T_2 (much shorter than tissue T_2 [2,5]) that further suppresses unwanted venous signals relative to tissue BOLD signals.

The challenges of ultra-high-field fMRI are also well described. Strong field perturbations near air–tissue or bone–tissue interfaces can cause significant distortion problems, as well as signal and resolution loss, for images acquired with echo-planar imaging (EPI) pulse sequences (the most common image acquisition method for fMRI). This problem is exacerbated for EPI acquisitions with read-out times that are long compared to the short T_2* at high fields (~25 ms in gray matter at 7T). Nonuniform coil sensitivity profiles also degrade the quality of high-resolution anatomical images, and thermal energy deposition by radio-frequency (RF) pulses [specific absorption rate (SAR)] can limit acquisition rates for spin echo (SE) EPI.

These issues are important because they often limit the volume that can be covered in fMRI studies at fields greater than 4 T. Human studies that have exploited the advantages of high-field fMRI for mapping structures such as cortical columns have generally been limited to restricted portions (a few centimeters) of the cortex [6,7]. One application that requires extended coverage and uniform sensitivity is

* Corresponding author. Departments of Psychology and Radiology, University of Minnesota, Minneapolis, MN 55455, USA. Tel.: +1 612 626 7607; fax: +1 612 626 2079.
E-mail address: caolman@umn.edu (C.A. Olman).

0730-725X/$ – see front matter © 2010 Elsevier Inc. All rights reserved.
doi:10.1016/j.mri.2010.06.001

retinotopic mapping. This paper uses a retinotopic mapping protocol to test the reliability and feasibility of 7T SE BOLD for fMRI applications studying responses distributed across multiple cortical regions. The posterior portions of the cerebral cortex contain many distinct representations of visual space — about a dozen visual field maps can be identified in a single retinotopic mapping experiment [8]. Successful retinotopic mapping requires (a) good sensitivity across a field of view (FOV) spanning both hemispheres and covering 5–10 cm in the anterior/posterior and superior/inferior directions, (b) a high-quality reference anatomy (in which gray and white matter can be automatically segmented such that the white-matter surface can be computationally inflated for clear depiction of visual field map organization) and (c) minimal distortion in the functional data to facilitate co-registration with the anatomical reference. Retinotopic mapping is therefore a good test of a technique's efficiency and accuracy spanning multiple cortical areas. To date, despite the growing number of sites doing neuroscience applications using fMRI at 7T, only one 7T retinotopic mapping experiment has been published [9] and that study was limited to gradient echo (GE) BOLD.

In this work, we investigate the feasibility of doing a stand-alone retinotopic mapping experiment with either GE or SE BOLD at 7T, using either a volume or a surface coil. We use the term *stand-alone* to describe fMRI studies in which the anatomical data are acquired during the same scanning session (i.e., with the same RF coil) as the functional data. For studies at 7T, this is a challenge because of the nonuniform RF sensitivity profiles — especially if a surface coil is used to maximize local BOLD sensitivity. However, normalization by simultaneously acquired proton density (PD) scans enables automated cortical segmentation of T_1-weighted anatomical images acquired at 7T [10], even images acquired with a surface coil. We apply this approach to the visualization of retinotopic mapping data.

In addition to demonstrating the feasibility of automated cortical surface definition using 7T anatomical images, our aims were to compare the sensitivity of 7T GE and SE BOLD data against 3T GE BOLD data with comparable resolution (1.8 mm isotropic) and to determine whether the visual area boundaries defined by the different techniques agreed. Because retinotopic boundaries are identified by fitting functional data that span several centimeters of cortex, the spatial characteristics of the retinotopic maps acquired with SE and GE BOLD are expected to be similar. Therefore, rather than attempting to demonstrate the superior spatial specificity of SE BOLD techniques, which has been amply demonstrated elsewhere, this study expects similar results from GE and SE BOLD techniques and tests whether the 7T SE technique can be applied across extended regions of cortex with sensitivity comparable to 3T GE BOLD. A thorough comparison of techniques across field strengths and BOLD techniques is not feasible in a single study because the sensitivity of both SE and GE BOLD techniques depends on resolution, with the optimal trade-off between thermal and physiological noise being reached at different voxel volumes (depending on the particular coil and pulse sequence used) and with SE BOLD techniques showing a particular advantage at high resolution (elimination of partial volume effects). Since the resolution dependence of the two techniques is well known [11], the data were all collected at a single voxel volume that is considered optimal for 3T GE BOLD [12].

2. Materials and methods

2.1. Subjects

Six subjects (two female, age 21 to 34) with normal or corrected-to-normal vision participated in the experiments. The experimental protocols conformed to safety guidelines for MRI research and were approved by the Institutional Review Board. Each subject participated in three or four scanning sessions, for the experiments described below, providing written informed consent after the nature of the experiments had been fully explained.

2.2. MRI systems

The 7T magnet (Magnex Scientific, UK) was equipped with a Siemens console (Erlangen, Germany) and a Siemens Avanto body gradient set capable of 40 mT/m and a maximum slew rate of 200 T/m/s. Two different RF head coils were used, as described below. The 3T scanner was a Siemens Trio system, with Avanto gradients and a 12-channel receive-only volume head coil.

2.3. Visual stimuli

Standard rotating and expanding checkered retinotopic mapping stimuli were generated in Matlab (MathWorks, Inc., Natick, MA). Stimuli covered 12.5% of the relevant visual field (22.5° of polar angle for the wedges, 1.5° of eccentricity for the rings). Subjects viewed four types of stimuli: expanding ring, contracting ring, clockwise rotating wedge and counterclockwise rotating wedge. Stimuli covered the visual field at a rate of 1 cycle every 24 s. Functional scans lasted 4 min 12 s, during which 10 1/2 cycles of one stimulus type were presented.

2.3.1. Experiment 1: GE BOLD with a volume coil at 7T

Subjects 1, 2 and 3 participated in this experiment. A 16-channel transmission line head array coil as described in Ref. [13] was used for both transmitting and receiving RF signal. Visual stimuli were presented with an Avotec fiber optic display system (Avotec, Stuart, FL, USA) mounted on the volume coil. Subjects participated in four scans, and in each scan one of the four stimulus types was presented. Anatomical images with 1-mm isotropic resolution were acquired with an MP-RAGE pulse sequence: TR=3000 ms, TI=1500 ms, TE=3.67 ms, 192 partition-encode steps, 256 phase-encode steps, 256 data points in the read direction, nominal flip angle=6°, T_{acq}=6 min 58 s. In addition, a PD-

weighted volume was acquired with parameters identical to the MP-RAGE acquisition except that the inversion preparation pulse and adjacent delays were removed (T_{acq}=3 min 14 s). In some subjects, the MP-RAGE and PD scans were acquired sequentially; in others, the acquisitions were interleaved in a single pulse sequence. Results from these two approaches were indistinguishable. Functional data were acquired using single-shot EPI in an oblique coronal orientation, perpendicular to the calcarine sulcus. Pulse sequence parameters were as follows: TE=24 ms, TR=3000 ms, flip angle=90°, FOV=235×115 mm, matrix size=128×64 with 6/8 partial Fourier acquisition (48 phase-encode lines), echo spacing=0.72 ms; 24 slices with a thickness of 1.8 mm covered 4.3 cm in the anterior/posterior direction. Field maps were acquired with a dual echo time field mapping sequence (ΔTE=1.02 ms), with 3 mm resolution. (Field map data were resampled using custom Matlab code for use with the FUGUE unwarping toolbox, see below.)

2.3.2. Experiment 2: SE BOLD with a surface coil at 7T

Subjects 1–6 participated in this experiment. A half volume coil was used for RF transmission and a small (6 cm) quadrature coil was used for reception [14]; these coils were actively decoupled during the acquisition. Visual stimuli were projected by a Sanyo (Sanyo North America Corporation, San Diego, CA, USA) projector with a custom zoom lens (NuView lens by Navitar, Rochester, NY, USA), housed outside the magnet room, onto a screen positioned behind the subjects' heads. Subjects viewed the screen through a mirror over their eyes. Subjects participated in 10 scans during one scanning session: 2 expanding rings, 2 contracting rings, 3 clockwise rotating wedges and 3 counterclockwise rotating wedges. Anatomical images with 1-mm isotropic resolution were acquired with an MP-RAGE pulse sequence: TR=3000 ms, TI=1500 ms, TE=3.67 ms, 160 partition-encode steps, 128 phase-encode steps, 256 data points in the read direction, nominal flip angle=6°. PD-weighted scans were also acquired, as with the volume coil data. Functional data were acquired using single-shot EPI in an oblique coronal orientation, perpendicular to the calcarine sulcus. Pulse sequence parameters were as follows: TE=50 ms, TR=3000 ms, flip angle=90°, FOV=230×115 mm, matrix size=128×64 with 6/8 partial Fourier acquisition (48 phase-encode lines), echo spacing=0.69 ms; 24 slices covered 4.3 cm in the anterior/posterior direction. Field maps were acquired, as in Experiment 1.

2.3.3. Experiment 3: GE BOLD with a surface coil at 7T

Subjects 4–6 participated in this experiment; the same coil and visual stimuli were used as for Experiment 2 (7T SE). Subjects viewed two scans: one with clockwise rotating wedges and one with counterclockwise rotating wedges. Functional data were acquired using single-shot EPI in an oblique coronal orientation, perpendicular to the calcarine sulcus. Pulse sequence parameters were as follows: TE=24 ms, TR=3000 ms, flip angle=90°, FOV=230×115 mm, matrix size=128×64 with 6/8 partial Fourier acquisition (48 phase-encode lines), echo spacing=0.72 ms; 24 slices covered 4.3 cm in the anterior/posterior direction. Field maps were acquired as in Experiments 1 and 2.

2.3.4. Experiment 4: GE BOLD with a volume coil at 3T

Subjects 3–6 participated in this experiment. Visual stimuli were projected by a Sanyo (Sanyo North America Corporation) projector with a custom zoom lens (NuView lens by Navitar), housed outside the magnet room, onto a screen positioned behind the subjects' heads. Subjects viewed the screen through a mirror over their eyes. Subjects viewed at least one scan of each of the four stimulus types. Anatomical images with 1-mm isotropic resolution were acquired with an MP-RAGE pulse sequence: TR=1900 ms, TI=700 ms, TE=5 ms, 176 partition-encode steps, 224 phase-encode steps, 256 data points in the read direction, nominal flip angle=7°, T_{acq}=7 min 18 s. Functional data were acquired using single-shot EPI in an oblique coronal orientation, perpendicular to the calcarine sulcus. Pulse sequence parameters were as follows: TE=31 ms, TR=2000 ms, flip angle=80°, FOV=168×105 mm, matrix size=96×60 with 6/8 partial Fourier acquisition (46 phase-encode lines), echo spacing=0.71 ms or 0.73 ms (depending on dB/dt limitations for the selected slice orientation); 24 slices covered 4.3 cm in the anterior/posterior direction. Field maps were acquired with ΔTE=2.46 ms.

2.4. Reference low-resolution retinotopic maps

All subjects had participated in a retinotopic mapping session prior to these experiments, using a standard parameter set: 3 mm isotropic voxels and 1500 ms TR. Because the stimuli for that experiment were wider (25% duty cycle instead of 12.5%), they were not included in the CNR comparison, but visual field boundaries from these maps were used for comparison against the new retinotopic mapping data.

2.5. Data pre-processing

All data were first processed with motion compensation [15] and high-pass temporal filtering (discarding Fourier components 4 cycles per scan or slower). Distortion compensation was performed using the PRELUDE and FUGUE tools provided with the fMRIB Software Library (http://www.fmrib.ox.ac.uk/fsl/).

2.6. Data analysis

The retinotopic mapping stimuli evoked traveling waves of activity across retinotopically organized visual cortex. For each voxel, we calculated the coherence (unsigned correlation) between the measured time series and the best-fit sinusoid [16,17]. The coherence is the amplitude of the stimulus-related Fourier component divided by the square

root of the integrated power spectrum. The phase of this best-fit sinusoid measures temporal delay of the fMRI responses relative to the beginning of the time series and, therefore, corresponds to either the polar angle component (for rotating wedge stimuli) or the eccentricity component (for expanding ring stimuli) of the retinotopic map. When using coherence as a measure of CNR, we limited the analysis to a band of V1 between approximately 2° and 6° eccentricity (full stimulus subtent was 10°). More foveal visual representations occupy more superficial locations in occipital cortex, and this restriction was imposed in order to minimize the confounding factor of differing BOLD sensitivity between the different experiments (the different coils had different sensitivity profiles; thus, the SNR differed significantly 3 or 4 cm into the occipital cortex, where high eccentricities are represented).

To average eccentricity scans together (for visualization and atlas fitting only; averaged data were not used for SNR or CNR calculations), the data from all scans were shifted forward in time 1 or 2 TRs to approximately compensate for the hemodynamic delay, and then the contracting ring scans were time-reversed (so that the last volume in the time-series data became the first, etc.). The shifted, time-reversed contracting ring scans were averaged with the shifted expanding ring scans to produce a single eccentricity map with no hemodynamic delay. A similar procedure was used for averaging the data from the clockwise and counterclockwise rotating wedges to produce polar angle maps.

2.7. Thermal and tissue SNR calculations

SNR values were estimated for individual voxels in individual scans (after motion compensation, but before temporal filtering or distortion compensation). Tissue SNR was calculated for each voxel as the mean intensity divided by the standard deviation through time (after removing the stimulus fundamental frequency and its first harmonic). The thermal SNR was estimated for each experiment by comparing voxel intensity against the average standard deviation (through time) in a volume of interest well outside the head. The noise region of interest (ROI) was selected above the head, since the read-out direction was superior/inferior, to avoid any image artifacts in the phase-encode direction.

2.8. Alignment of functional data and volume anatomy

The motion-compensated, distortion-compensated EPI series were aligned directly to the 3D MP-RAGE volume anatomy acquired during the scanning session. Automatic image alignment [15] between EPI data and 3D anatomical scans was performed after inverting the voxel intensities in the EPI image to match the T_1 contrast of the inversion-prepared (MP-RAGE) volume anatomy. This alignment information was used for several data-space transformations. For surface-based visualization, functional activation maps (coherence and phase) were resampled into matrices with 1-mm resolution to match the source data for the cortical surfaces. Gray-matter ROIs defined on flattened cortical surfaces were also translated to the high-resolution anatomical images and then to each of the functional data sets to extract data for CNR comparisons.

2.9. Segmentation of volume anatomies and definition of cortical surfaces

Gray- and white-matter voxels were defined in both the whole-brain and partial-brain MP-RAGE volume anatomies using SurfRelax [18]. The extracted white-matter surfaces were then inflated and flattened for visualization of functional organization. To compensate for strong variation in white-matter intensity in the original MP-RAGE images acquired at 7T, the T_1-weighted MP-RAGE volume was divided by the corresponding PD-weighted scan [10], after the two volumes were aligned with each other to compensate for any motion between the two acquisitions (in the case of data acquired in a non-interleaved manner).

For cortical surface reconstruction of partial brain anatomies acquired with a surface coil, we compared both manual and automatic generation of ventricle masks and hemisphere boundary definitions. Manual masking required 20 to 30 min per brain. Automatic generation of the mask required the posterior anatomical data to be zero-padded to create a volume in which the posterior anatomy had the correct orientation and occupied the correct position in a full brain-sized volume. Whole-brain templates in the software package could then fit the posterior horn of the lateral ventricle and generate boundaries for left and right hemispheres. Both processes produced similar results. Once ventricles were filled and hemisphere boundaries were defined (manually, in the final analysis), surface definition and inflation were automatic. For all anatomical data sets, about an hour of manual correction was required to correct segmentation errors on isolated gyri in posterior cortex.

2.10. Atlas warping to define retinotopic area boundaries

Software distributed with the Stanford Matlab tools for retinotopic data analysis (http://white.stanford.edu/~sweta/VistaLab/Manual/mrloadret.html) was used for automated visual area boundary fitting [19]. Briefly, quadrilaterals representing the approximate locations of V1, V2v, V2d, V3v and V3d were defined manually, and then the phase maps generated from this template were warped to fit the actual phase data. To characterize the spatial offset between different experiments' estimates of the visual area boundaries, we calculated the average distance between second-order polynomial fits to each of the identified boundaries.

3. Results

3.1. Tissue classification in anatomical images

Like many neuroscience applications, retinotopic mapping requires segmentation of the cortical gray matter and

surface-based visualization in order to quantify results. Unwanted signal intensity variations arise from nonuniform coil sensitivity, as well as from PD and T_2* weighting; removing these unwanted signal variations is crucial to the success of automated surface reconstruction from anatomical data sets at 7T (Fig. 1). 3D GE PD-weighted images can be used to remove (divide out) signal intensity variations in T_1-weighted 3D MPRAGE images while preserving the underlying T_1 contrast [10]. After the T_1 normalization step, we found no systematic differences in the segmentation and reconstruction of surfaces from whole-brain anatomies acquired at 3T and 7T. For both 7T and 3T anatomical data sets, the defined surfaces needed some manual editing to correct regions where the algorithm failed to identify narrow bands of white matter or where sulci were not deep enough.

Because many high-field/high-resolution experiments use a surface RF coil to improve the local SNR or to reduce SAR for SE BOLD experiments, an important question for this study was whether cortical surfaces can be reconstructed automatically from partial-brain anatomies acquired with a surface coil. While surface coils provide superior SNR in superficial brain regions, intensity falls off rapidly with distance from a surface coil, making it difficult to acquire useful anatomical images in the same scanning session. Fig. 2 illustrates the process of reconstructing a posterior cortical surface from surface-coil data (see Materials and methods for details). Figs. 4, 5 and 7 show surfaces successfully extracted from anatomies acquired with a surface coil.

3.2. CNR and SNR comparisons

Our first interest was to compare, within the practical limitations of using different hardware at different field strengths[1], the sensitivity of the 3T GE BOLD data against the 7T SE and GE BOLD data. Average Fourier spectra for the different experiments are shown in Fig. 3. Strong modulation at the stimulus frequency (10 cycles per scan) is clear for all experiments. Because the stimulus was presented with a 12.5% duty cycle, significant signal modulation is also present at the first harmonic for all scans. Modulation was, on average, strongest for the 7T GE BOLD [1.9±0.11% (S.E.M.), across 12 hemispheres] and comparable for the 7T SE BOLD (1.3±0.08%, 12 hemispheres) and the 3T GE BOLD (1.4±0.13%, 8 hemispheres).

BOLD sensitivity is determined not only by the amplitude of the modulation (contrast) but also by amplitude of signal intensity fluctuations not related to the experiment design (noise). CNR was therefore characterized for each experiment by the average coherence in V1 ROIs (all V1 gray matter between 2° and 6° eccentricity) defined separately for each subject. Average coherence for the 3T GE BOLD experiments was 0.25 (S.D.=0.04), and for the 7T GE BOLD experiments, it was 0.41 (±0.06, Fig. 3B). The average coherence for the SE data was 0.23 (±0.06).

The greatest variability, across subjects and between hemispheres in individual subjects, was in the coherence of the SE data. To explain this variability, we quantified both physiological and thermal SNR for each experiment. The tissue SNR metric measures total fluctuation in intensity, whether it arises from thermal noise or physiological noise sources like respiration. Stimulus coherence correlated significantly with tissue SNR for all experiments: a linear relationship between the two metrics was observed regardless of field strength or modality (Fig. 3B).

For the experiments with lower coherence and tissue SNR (3T GE BOLD and 7T SE BOLD), tissue and thermal noise were correlated, demonstrating a linear relationship in this low SNR regime. A linear fit (with forced zero intercept) to the 3T GE and 7T SE data points yielded a slope of 2.1, which is in good agreement with the 2:1 physiological-to-thermal noise ratio reported in Ref. [11]. For the 7T GE data, however, tissue SNR was largely independent of thermal SNR (dark blue dots, Fig. 3C). This is the expected result if physiological noise (e.g., fluctuations due to respiration, vasoregulation, pulsatile motion of the brain related to the cardiac cycle) limits the BOLD sensitivity in a regime where physiological fluctuations are large relative to thermal noise [20].

3.3. Comparison of visual field maps

A pair of eccentricity and polar angle maps shown in Fig. 4 (left hemisphere of Subject 2) illustrates the retinotopic organization of the region of posterior occipital cortex that was covered in all of our experiments. The organization of these maps, acquired in this case with SE BOLD at 7T, is similar to retinotopic organization reported in the literature; visual areas are labeled in keeping with Wandell et al. [8]. Data are shown with no smoothing. The limit of the coverage is indicated by a black dashed line. Because of this limited coverage, imposed by our use of a surface coil to avoid SAR limitations in the SE experiments, we did not map or label visual areas other than those sharing the posterior foveal representation with V1.

The cortical organization measured with GE BOLD and SE BOLD was similar, as illustrated for one hemisphere from each of the first three subjects in Fig. 5. The 7T GE BOLD maps (top row) were acquired in 9 min (average of 2 scans); the 7T SE BOLD maps (bottom row) were acquired in 27 min (average of 6 scans). Importantly, the functional data sets are each visualized on anatomical surfaces reconstructed from scans acquired during the same scanning session. Most notably, the SE BOLD maps are shown on cortical surfaces reconstructed from anatomical images acquired with a surface coil.

[1] Pulse sequence details such as sampling bandwidth were not precisely matched between the two scanners to make a fair comparison of imaging SNR; pulse sequences were simply optimized for the hardware at each scanner. There were significant differences in the design of the RF coils at the different scanners, which can also affect the imaging SNR. Repetition times were 2 and 3 s at 3T and 7T, respectively, to accommodate the longer T_1 at 7T.

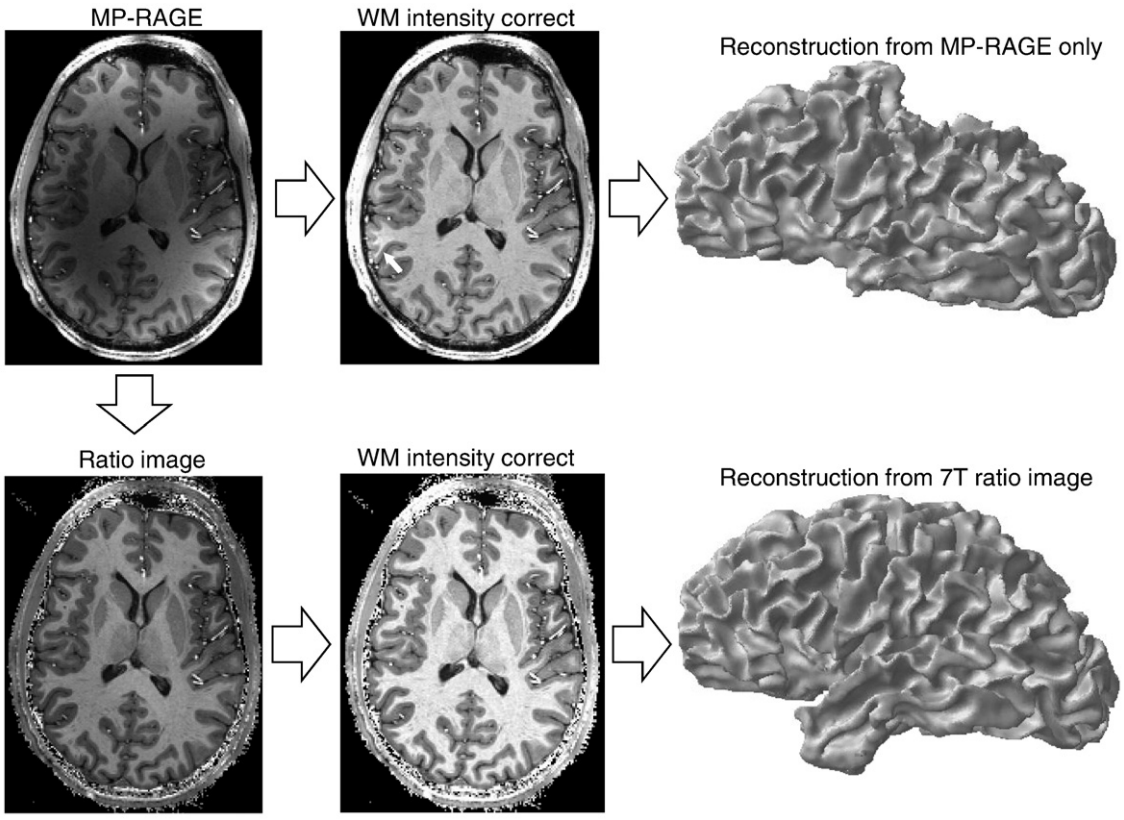

Fig. 1. Correction of intensity inhomogeneities allows for automated surface definition from high-field anatomical data. Top left: axial section from a T_1-weighted image (1 mm isotropic resolution) acquired with the 16-channel volume coil. Pattern of intensity nonuniformity is typical for 7T images acquired with transmit/receive coils, although systems with a separate transmit coil may produce less severe nonuniformities that may enable automated reconstruction without PD normalization. Top middle: standard surface reconstruction software packages have a first-pass white-matter intensity correction stage (WM intensity correct), in which a coarse segmentation provides a low spatial frequency intensity filter. The nonuniformities are so strong, however, that these algorithms fail (white arrow). Top right: incomplete white-matter definition makes it impossible to define a cortical surface (this segmentation was accomplished with SurfRelax; similar results were obtained with FreeSurfer). Bottom left: division by PD scan (Ratio image) reduces intensity variations in white matter. The division generates some high-intensity noise at the perimeter of the brain, which can interfere with skull stripping but does not interfere with automated white-matter surface definition. Bottom middle: corrected and normalized image, from which white matter can be segmented to define a full cortical surface (bottom right). About an hour of manual editing was required to remove residual errors in white-matter definition for superior temporal and inferior frontal regions; the same problems are commonly seen in 3T acquisitions.

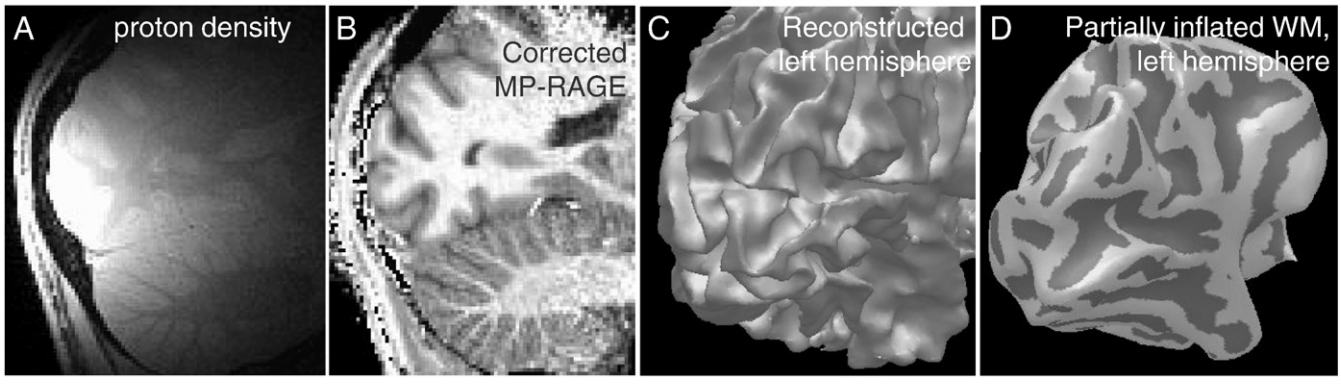

Fig. 2. Correction of intensity inhomogeneities enables automated surface definition and inflation for partial brain anatomical data acquired at 7T. (A) A "proton density" scan shows the sensitivity profile of the surface coil, positioned here to cover early visual areas. (B) The raw T_1 anatomy has the expected nonuniformity in intensity, but the corrected image shown here (MP-RAGE divided by PD) has uniform contrast throughout posterior cortex, up to the limit where coil SNR is insufficient. (C) The cortical surface is reconstructed by finding the boundary between white matter and gray matter. The intensity-based algorithm relies on uniform white-matter intensity throughout the cortical region. (D) The final product is an inflated white-matter surface. Light gray shading indicates regions of positive curvature (gyri); dark gray indicates negative curvature (sulci).

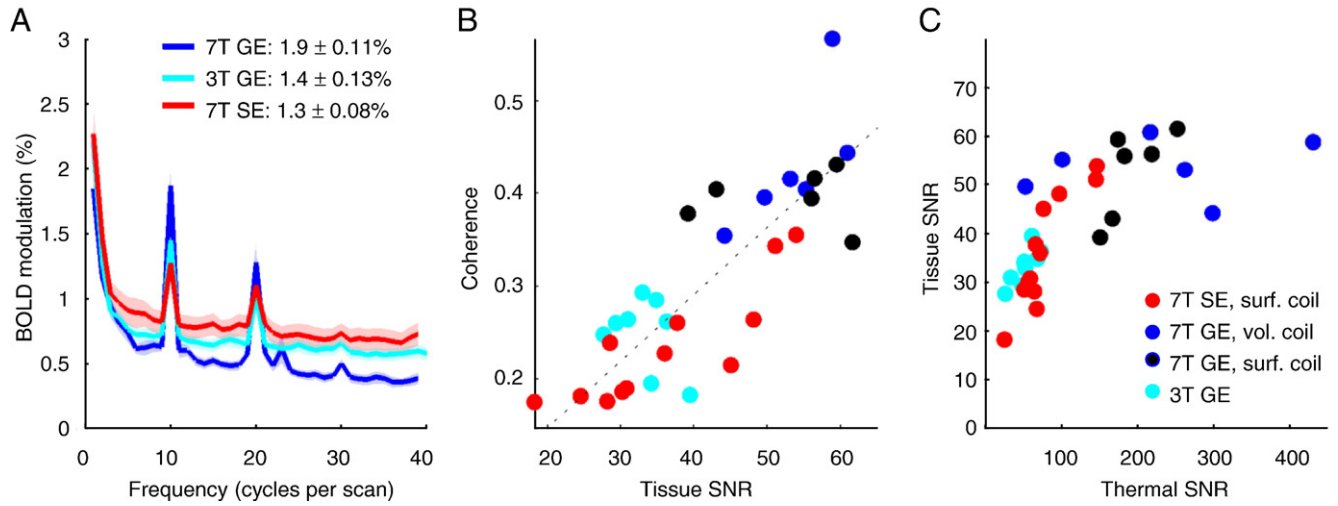

Fig. 3. Fourier spectra and CNRs estimated from the retinotopic mapping experiment. (A) Average amplitude spectra for all 1.8-mm acquisitions. All subjects participated in the 7T mapping sessions (7T GE data for Subjects 1–3 were acquired with a volume coil, 7T GE data for Subjects 4–6 were acquired with a surface coil; all 7T SE data were acquired with a surface coil); Subjects 3–6 participated in the high-resolution 3T mapping session. Data for each experiment are averaged in ROIs defined as subsets of V1 from approximately 2° to 6° eccentricity (an average of 345 voxels per hemisphere). BOLD contrast was characterized by the amplitude of modulation at 10 cycles per scan. (B) Average tissue SNR (mean intensity divided by standard deviation through time for each voxel) was calculated for each hemisphere of each subject. Stimulus coherence is the unsigned correlation between the BOLD data and a sinusoid at 10 cycles per scan. A strong linear correlation was observed between coherence and tissue SNR (dotted line). (C) Thermal SNR was calculated as the mean voxel intensity divided by average standard deviation (through time) in a noise ROI defined outside the brain.

To quantify the similarity of the retinotopic maps acquired with GE BOLD and SE BOLD at 7T, we aligned the functional data from all of the experiments in each subject to a single anatomy for that subject and used an automated atlas-fitting algorithm to compare visual area boundaries for V1, V2 and V3. The results of these comparisons are shown in Fig. 6. As a visual map standard, we used low-resolution 3T retinotopic mapping data [labeled 3T ref (3 mm) in Fig. 6] acquired previously for each subject. We then quantified variation in visual area size estimates due

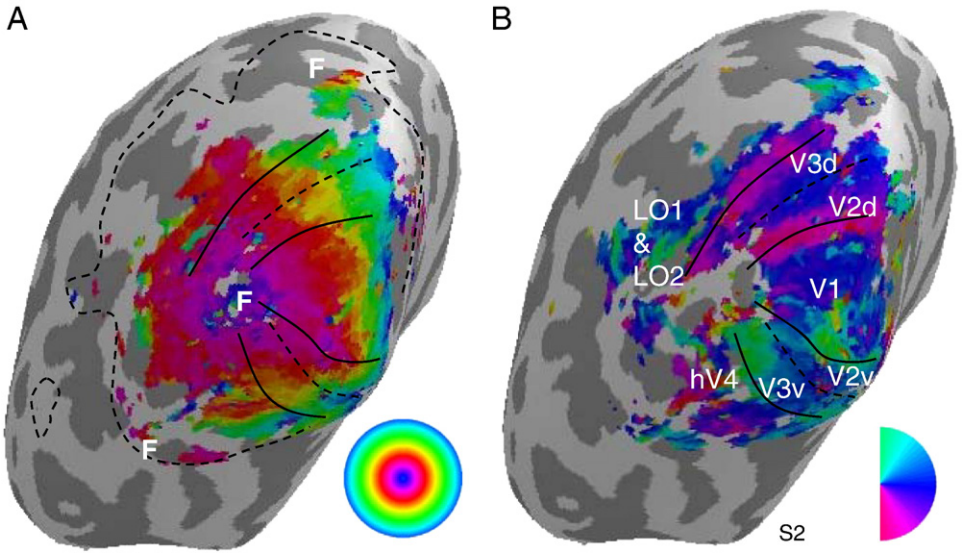

Fig. 4. SE retinotopic data from one subject illustrates the coverage achieved in this experiment, as well as the basic organization of early visual areas. The phase of the stimulus-related Fourier component (encoding visual field location, as indicated by inset legends) is visualized on inflated cortical surfaces reconstructed from anatomical images acquired with a surface coil. (A) The eccentricity map is the average of four scans. No smoothing was used for the functional data; data are shown for voxels with coherence greater than 0.3 ($P<.001$, uncorrected). Dashed line indicates extent of coverage for functional data; coverage was sufficient for early visual areas but was not sufficient to fully visualize maps sharing foveal representations (marked with F) on the dorsal and ventral surfaces of the brain. (B) Early visual areas are marked on the polar angle map derived from the rotating wedge functional scans.

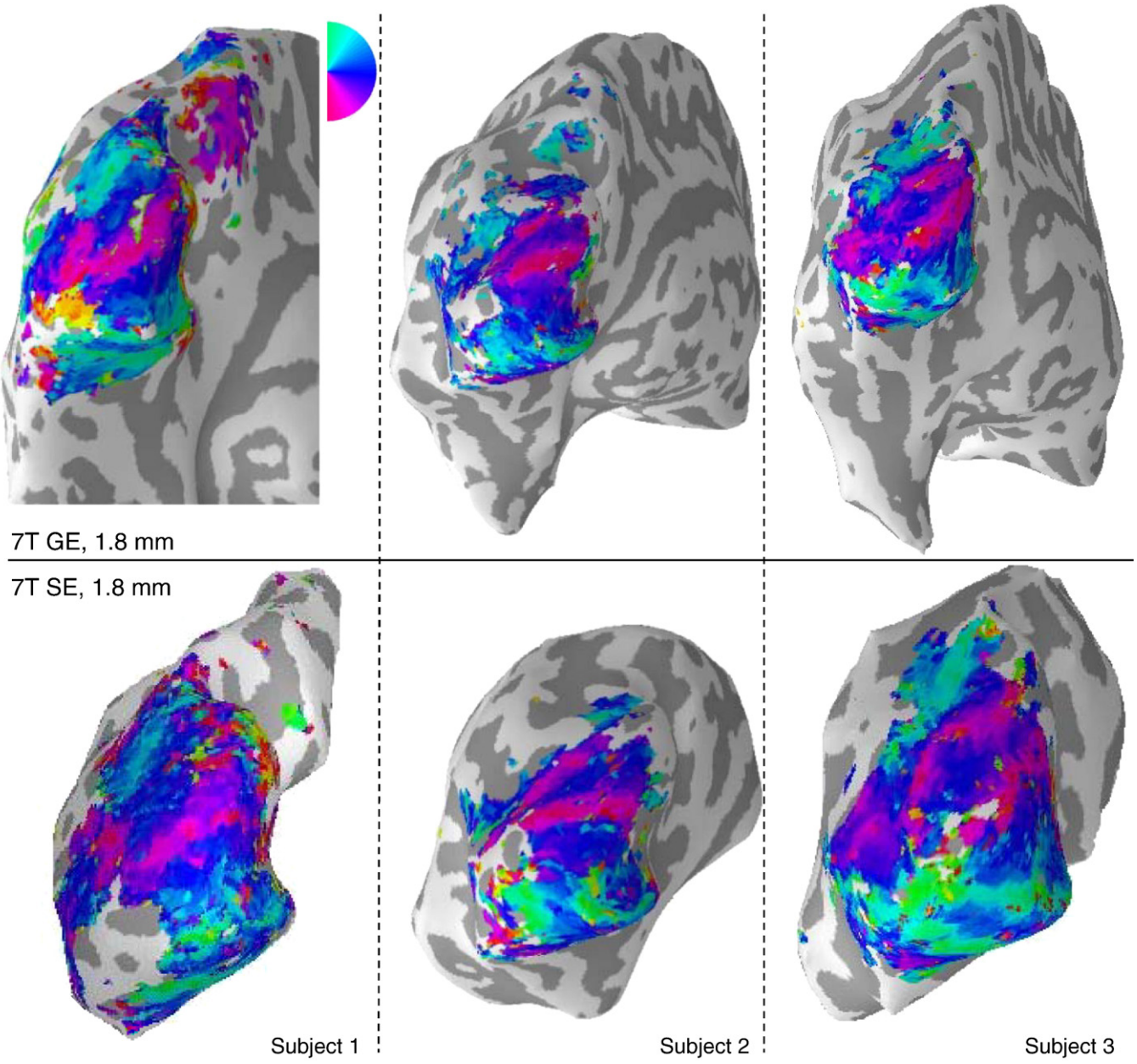

Fig. 5. Retinotopic maps for three hemispheres. Top row: retinotopic maps acquired with GE BOLD at 7T (1.8-mm resolution, average of two 4-min scans), visualized on whole-brain cortical surfaces reconstructed from anatomical images acquired with a volume coil at 7T. Bottom row: retinotopic maps acquired with SE BOLD (1.8-mm resolution, average of six 4-min scans), visualized on partial-brain cortical surfaces acquired with a surface coil. (To the extent allowed by the different shapes of the different inflated hemispheres, the partial hemispheres are viewed from the same angle as the complete hemispheres, but the perspective could not be perfectly matched.) For all data sets, functional data from voxels with coherence >0.30 are visualized on inflated surfaces, except for the SE data from Subject 1, for which voxels with coherence >0.25 are shown. Missing data due to errors in alignment between functional and anatomical data are apparent as holes in the color overlay.

to variability of boundaries located on the horizontal and vertical meridia. While there was a trend toward smaller V1 estimates in the SE BOLD data, this was driven by data from Subject 3 (the most variable of the six subjects for which we did atlas fitting, shown in Fig. 6) and was not statistically significant across the data set (two-tailed paired t test, P=.31, n=12 hemispheres). The total size of V1, V2 and V3 (combined) was also not different between the 7T experiments and the 3T reference data.

In addition to measuring the size of the early visual areas mapped by the 7T GE and SE techniques, we quantified boundary location and the degree of overlap between the 7T data and the 3T reference data (Fig. 6, right panels). For the SE BOLD data, overlap was best for V1 (90%) and slightly lower (79%) for the quarterfield representations of V2 and V3. The GE data also showed good overlap for V1 (93%), but there was a trend toward decreased overlap in V2v and V3v, with overlap as low as 73% for ventral V3. As

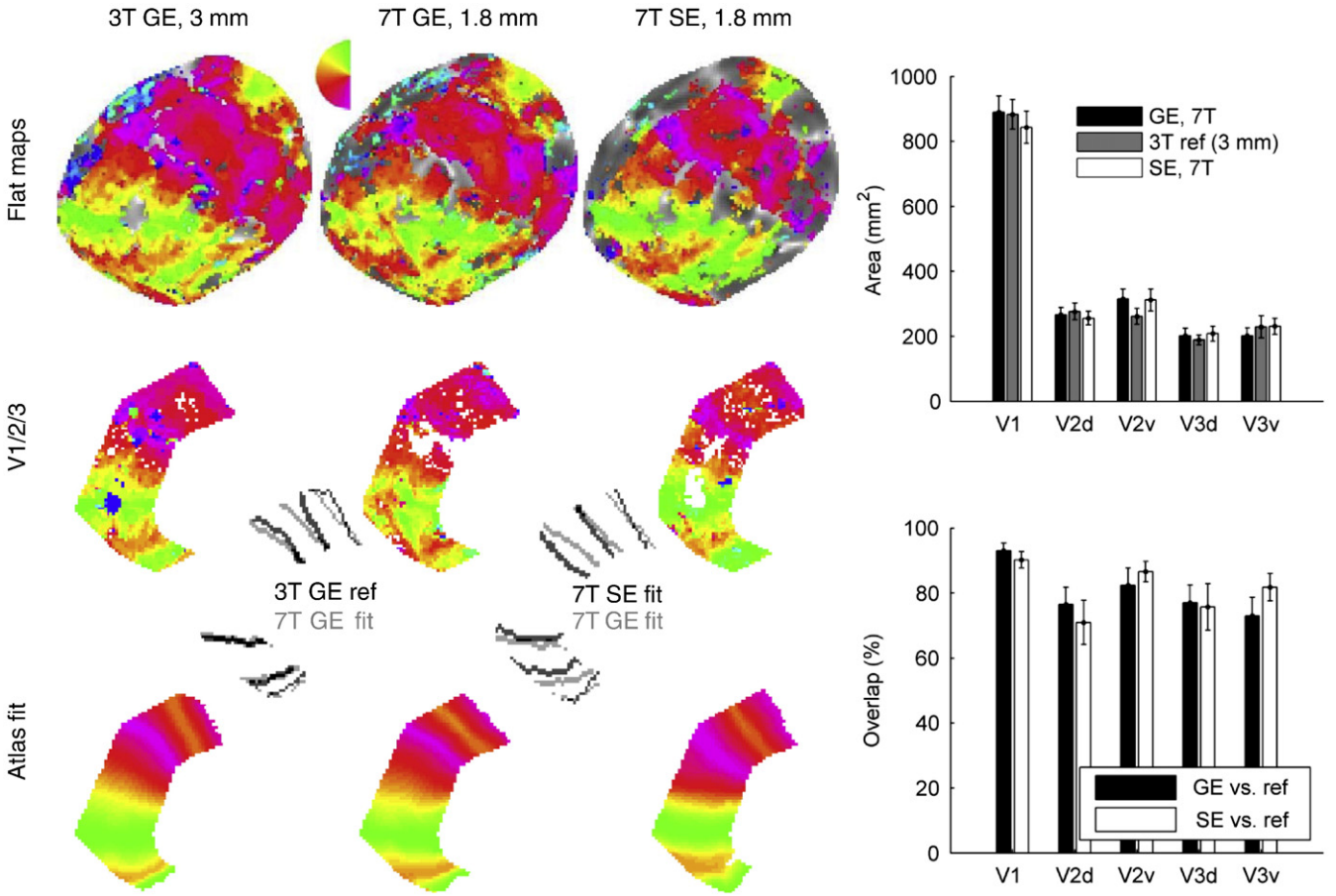

Fig. 6. Atlas fitting quantifies visual area boundaries. At left, atlas fitting is illustrated for Subject 3, right hemisphere. Top row: data are visualized on flat patches from the same (3T) reference anatomy. Because not all of the subjects who participated in the 7T studies participated in the 3T high-resolution mapping study, 3T GE BOLD retinotopic mapping data with 3-mm resolution is used as the reference. Middle row: sub-region of V1/2/3 extending from approximately 2° to 6° eccentricity, for which atlas fitting was performed. Bottom row: phase atlases created for each hemisphere after warping to match the phase data. Phase reversals in these warped atlases define visual area boundaries, which are indicated by the inset gray lines. A comparison between 3T and 7T GE map boundaries is shown in the left inset; a comparison of 7T GE and SE map boundaries is shown in the right inset. The bar chart at the upper right indicates the average area (n=12 hemispheres, error bars indicate S.E.M.) of the restricted eccentricity band for each visual area, for each modality. The bar chart on the lower right indicates, for the 7T GE and SE data sets, what percentage of voxels in each visual area were also contained in the corresponding visual area defined by the 3T reference data.

discussed below, these data were acquired with a single-shot pulse sequence, thereby increasing the severity of susceptibility-induced artifacts, which are more pronounced in ventral cortical regions.

We also compared the locations of the visual area boundaries automatically defined for each data set in each subject. The average distance between a boundary estimated from the low-resolution 3T reference data and the high-resolution 7T GE BOLD data was 2.85±0.32 mm (S.E.M., 41 out of 48 V1/V2 and V2/V3 boundaries, with 7 eliminated because of poor linear fits to the boundary). The average distance between a boundary estimated from the low-resolution 3T reference data and the high-resolution 7T SE BOLD data was 3.28±0.35 mm. Comparing the 7T GE BOLD boundaries against the 7T SE BOLD boundaries, we found an average displacement of 2.32±0.33 mm. A similar comparison between maps acquired with 3T GE BOLD with 3- and 1.8-mm resolution found the same magnitude of displacement (2.7±0.4 mm), suggesting that the differences between visual area boundaries defined at 7T and 3T are due to imperfections in alignment and distortion compensation, rather than field strength.

3.4. Distortion compensation

One of the known practical limitations for functional MRI at 7T is the increased severity of distortion due to susceptibility-induced field gradients. The high-resolution functional data acquired on the 7T scanner in this study used large image matrices (128×64) acquired in a single shot (i.e., not taking advantage of segmentation or parallel imaging to reduce the read-out time). Therefore, the read-out time was longer than ideal, given the short T_2* and magnitude of the magnetic field inhomogeneities at 7T (which lead to blurring and image distortions, respectively). Distortion compensation in the functional data acquired at

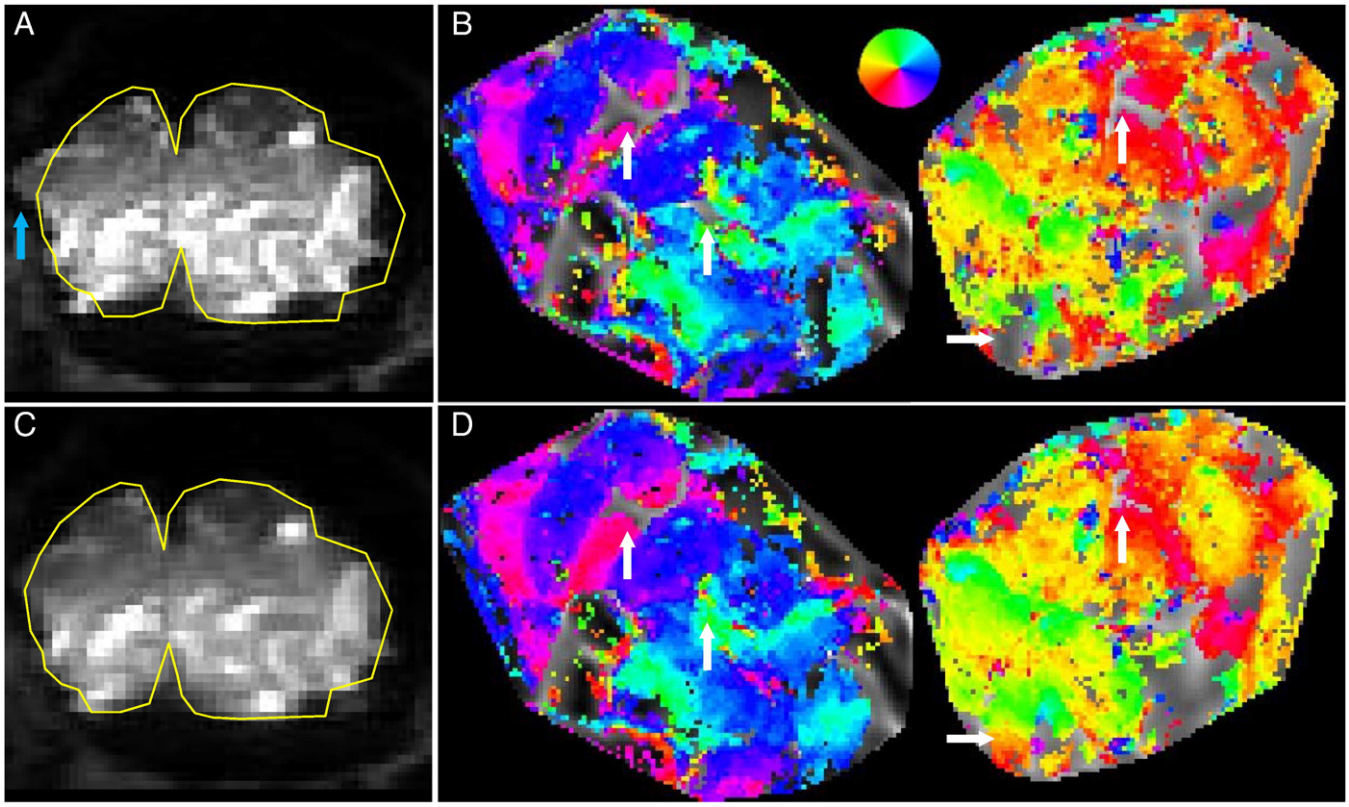

Fig. 7. Correction of image distortion due to field inhomogeneities improves visualization of retinotopic maps from functional data acquired at 7T. (A) The raw distorted EPI image; yellow reference line shows true brain boundary as measured by anatomical data. Blue arrow indicates a region of particularly strong distortion. (B) Left and right hemisphere maps from a single subject, before distortion compensation. Functional data are shown on flattened cortical patches; legend in the middle indicates color code for visual field position. (C) Residual distortion is still apparent in distortion-compensated images, as the "corrected" EPI data still do not perfectly match the anatomical reference. (D) Functional data from the distortion-compensated images is nevertheless more consistently represented on the reconstructed cortical surface, both because of improved alignment between functional and anatomical data and better fidelity of shape. White arrows indicate regions of particular improvement.

7T was therefore necessary to achieve consistently good alignment between functional and anatomical data (Fig. 7). Strong local perturbations in the field at the edges of the brain cannot be corrected with even high-order shims [21], producing significant distortion along the edges of the cortex (Fig. 7A). These localized errors create regions where data are misaligned and cannot be visualized on the cortical surface (white arrow, Fig. 7B). Field-map-based distortion compensation during post-processing corrected many of these errors (Fig. 7C and D), although some significant displacements still remained due to imperfect alignment between the field map and the EPI data or limitations of the unwarping algorithm.

4. Discussion

This study had two primary goals: to demonstrate the feasibility of stand-alone functional MRI studies at 7T and to compare the efficacy of SE and GE BOLD at 7T against GE BOLD at 3T. To the best of our knowledge, this article includes the first published utilization of automatic cortical surface definition from 7T anatomical data (surface and volume coil acquisitions), a capability that enables not only the mapping of multiple visual field representations at 7T but also many other studies of neural coding that require the visualization of extended patterns of neural activity on the cortical surface. With this capability, it is not necessary to acquire separate data sets (at lower field strength) for anatomical reference images for surface-based or other analyses that require knowledge of the cortical geometry. While no automated cortex segmentation program will generate a segmentation that is error-free, the high-quality starting point enabled by the PD normalization as demonstrated in this study represents a significant improvement in efficiency for high-field studies.

Our second goal was twofold: to compare the sensitivity of 7T SE and GE BOLD fMRI against 3T GE BOLD and to compare the spatial characteristics (visual area boundaries) of the resulting maps. One limitation to using SE BOLD in many functional imaging experiments is the reduction in CNR, relative to GE BOLD. This is similar to the challenge of using cerebral blood flow techniques to perform retinotopic mapping [22]. In the comparison of 7T SE

BOLD and 3T GE BOLD data sets, we found comparable CNR. The range of CNR values we measured for the SE BOLD experiments was large. Some data had CNR as low as the 3T GE BOLD and some data had CNR as high as the 7T GE BOLD. This variability is most likely due to the fact that the SE BOLD data were acquired with a surface coil, which means that SNR is more spatially variable and sensitive to the precise position of the subject's head. Indeed, thermal noise (image SNR) and physiological noise (tissue SNR) were well correlated for the SE BOLD data, suggesting a strong dependence of CNR on image quality. Similarly, the design of the particular volume coil used for some of the 7T GE BOLD studies was such that the coil sensitivity had a strong spatial dependence: although sensitivity did not fall off as strongly with distance from the coil (depth in the brain), the sensitivity is 2× greater for superficial gray matter than for deep cortical tissue. Therefore, a large portion of the scatter in the SNR of the 7T GE data, even the data acquired with the volume coil, can likewise be explained by the particular geometry of the subjects' head.

The CNR of the 7T GE BOLD data was almost twice that of the 3T GE BOLD data, an increase in CNR that would be expected if thermal noise rather than physiological noise limits the CNR of the 3T GE BOLD data [23]. The thermal SNR of the 7T GE BOLD data was, however, more variable than the 3T GE BOLD data, even though both were acquired with volume coils. The design of the transmit/receive volume coil has a much more variable sensitivity profile (Fig. 1) than the receive-only head coil used at 3T; hence, the 7T data were strongly sensitive to the particular position and cortical geometry of the individual subject.

A recent report by Hoffmann et al. [9] compared SNR at different resolutions for 3T and 7T GE BOLD. Our findings are consistent with these, notably the SNR advantage of 7T, which enables BOLD experiments with the same sensitivity to be executed in a shorter time. The present study extends the comparison to include SE BOLD. In general, the exclusion of large veins from the SE BOLD signal significantly reduces the CNR of SE BOLD relative to GE BOLD, and it is important to demonstrate that at moderate resolutions, the CNR of SE BOLD is still comparable to what can be achieved with GE BOLD at 3T. Therefore, we find that high-resolution applications measuring BOLD responses in multiple cortical areas can take advantage of either the increased magnitude of the GE BOLD response at 7T or the increased spatial specificity of the SE BOLD response. Previous studies have also found that the CNR of SE BOLD actually increases with decreasing voxel size [11], suggesting an increased advantage of 7T SE BOLD for very high-resolution mapping studies.

The data reported here have a larger FOV than previously reported 7T SE BOLD studies [6,24,25], but the data were acquired with a surface coil and therefore do not investigate the organization of higher visual areas along the dorsal or ventral streams. For example, we did not acquire functional data in the more anterior ventral visual areas such as VO-1,2 [26–28] because our 1.8-mm acquisitions had limited volume coverage (dashed line, Fig. 3A). We do note, however, that the organization of cortex ventral to V3v does not always appear the same. For example, in the left hemisphere maps of Subject 3 (Fig. 5), there appears to be a full hemifield representation ventral to V3v, consistent with some reports [8]. The 7T SE right hemisphere maps of the same subject show the same hemifield organization when visualized on a cortical surface defined from the 7T surface-coil data (Fig. 7), but the 7T SE data do not show the same hemifield organization when visualized on the cortical surface defined from the 3T anatomy (Fig. 6). This suggests that slight errors in segmentation or alignment are masking the true cortical organization. Because we were working with single-shot data with significant distortion and variability on the ventral cortical surface, with a slice prescription not optimized to fully cover the ventral visual representations, we did not pursue quantification of the organization ventral visual areas anterior to V3v. However, further experiments will investigate the causes of the variability we observed on the ventral cortical surface.

One significant improvement over the data acquired in this study would be the use of parallel imaging [29], in part to improve the image resolution, but more importantly to reduce the read-out time for single images and thereby minimize the field inhomogeneity-induced distortions, which in this study were significant and not fully corrected. The SE BOLD data set was acquired with a surface coil to avoid SAR limitations on the number of slices that could be acquired per second. However, B1 shimming [30] can improve the efficiency of volume coil acquisitions at 7T to enable extended coverage with SE BOLD sequences, taking advantage of parallel imaging. Likewise, for this study, the GE BOLD data were acquired without parallel imaging to match the SE data set, but this is not an inherent limitation. For example, whole-brain coverage with 1.5-mm isotropic resolution and 1.5-s TRs [31] has recently been reported.

In conclusion, we found that visual area boundaries were comparable whether measured with 3T GE BOLD, 7T GE BOLD or 7T SE BOLD. Current technology limits the total FOV that can be covered with SE techniques (relative to SE techniques) because of SAR considerations, but even with those limitations, coverage of multiple visual areas is feasible. The finding that the sensitivity of SE BOLD at 7T is comparable to GE BOLD at 3T (for the moderately high-resolution of 1.8 mm) establishes the feasibility of using SE techniques to study distributed information processing within and between cortical areas. Retinotopic maps were also of equal quality regardless of whether they were visualized on cortical surfaces defined from reference anatomies acquired at 3 or 7T, with a volume coil or with a surface coil.

Acknowledgments

The authors would like to thank Jay Hegde and Serena Thompson for their comments on the manuscript and Jim Porter for his expertise with Free Surfer. This work was also supported by NIH grants R01 MH070800 and R01 EB000331 to E. Yacoub, the BTRR P41 008079 grant at the Center for Magnetic Resonance Research and the CMRR/Mayo NCC grant P30 NS057091, as well as funding from the Keck Foundation and MIND Institute.

References

[1] Ugurbil K, Adriany G, Andersen P, et al. Ultrahigh field magnetic resonance imaging and spectroscopy. Magn Reson Imaging 2003;21 (10):1263–81.
[2] Yacoub E, Shmuel A, Pfeuffer J, et al. Imaging brain function in humans at 7 Tesla. Magn Reson Med 2001;45(4):588–94.
[3] Yacoub E, Duong TQ, Van de Moortele PF, et al. Spin-echo fMRI in humans using high spatial resolutions and high magnetic fields. Magn Reson Med 2003;49:655–64.
[4] Vaughan JT, Garwood M, Collins CM, et al. 7T vs. 4T: RF power; homogeneity; and signal-to- noise comparison in head images. Magn Reson Med 2001;46:24–30.
[5] Thulborn KR, Waterton JC, Matthews PM, Radda GK. Oxygenation dependence of the transverse relaxation time of water protons in whole blood at high field. Biochimica et Biophysica Acta—General Subjects 1982;714(2):265–70.
[6] Yacoub E, Shmuel A, Logothetis N, Ugurbil K. Robust detection of ocular dominance columns in humans using Hahn spin echo BOLD functional MRI at 7 Tesla. NeuroImage 2007;37(4):1161–77.
[7] Yacoub E, Harel N, Ugurbil K. High-field fMRI unveils orientation columns in humans. Proc Natl Acad Sci U S A 2008;105(30): 10607–12.
[8] Wandell BA, Brewer AA, Dougherty RF. Visual field map clusters in human cortex. Phil Trans R Soc Lond B 2005;360:693–707.
[9] Hoffmann MB, Stadler J, Kanowski M, Speck O. Retinotopic mapping of the human visual cortex at a magnetic field strength of 7T. Clin Neurophysiol 2008;120(1):108–16.
[10] Van de Moortele PF, Auerbach EJ, Olman CA, Yacoub E, Ugurbil K. T1 weighted brain images at 7 Tesla unbiased for proton density, T2 contrast and RF coil receive B1 sensitivity with simultaneous vessel visualization. NeuroImage 2009;46(2):432–46.
[11] Yacoub E, Van de Moortele PF, Shmuel A, Ugurbil K. Signal and noise characteristics of Hahn SE and GE BOLD fMRI at 7 T in humans. NeuroImage 2005;24(3):738–50.
[12] Bodurka J, Ye FQ, Petridou N, Murphy K, Bandettini PA. Mapping the MRI voxel volume in which thermal noise matches physiological noise — implications for fMRI. NeuroImage 2007;34:542–9.
[13] Adriany G, Van de Moortele PF, Wiesinger F, et al. Transceive stripline arrays for ultra high field parallel imaging applications. Proceedings of the 11th ISMRM Scientific Meeting, Toronto, Canada; 2003.
[14] Adriany G, Pfeuffer J, Yacoub E, et al. A half-volume transmit/receive coil combination for 7 Tesla applications. Proceedings of the 9th Scientific Meeting and Exhibition, International Society for Magnetic Resonance in Medicine, Glasgow; 2001 [abstract 1097].
[15] Nestares O, Heeger DJ. Robust multiresolution alignment of MRI brain volumes. Magn Reson Med 2000;43:705–15.
[16] Bandettini PA, Jesmanowicz A, Wong EC, Hyde JS. Processing strategies for time-course data sets in functional MRI of the human brain. Magn Reson Med 1993;30(2):161–73.
[17] Engel SA, Glover GH, Wandell BA. Retinotopic organization in human visual cortex and the spatial precision of functional MRI. Cerebral Cortex 1997;7:181–92.
[18] Larsson J. Imaging vision: functional mapping of intermediate visual processes in man. Stockholm, Sweden: Karolinska Institutet; 2001.
[19] Dougherty RF, Koch VM, Brewer AA, Fischer B, Modersitzki J, Wandell BA. Visual field representations and locations of visual areas V1/2/3 in human visual cortex. J Vis 2003;3:586–98.
[20] Triantafyllou C, Hoge RD, Krueger G, et al. Comparison of physiological noise at 1.5T, 3T and 7T and optimization of fMRI acquisition parameters. NeuroImage 2005;26:243–50.
[21] Clare S, Evans J, Jezzard P. Requirements for room temperature shimming of the human brain. Magn Reson Med 2006;55(1): 210–4.
[22] Liu AM, Hu X. Retinotopic mapping of human visual cortex using arterial spin labeling. Proceedings of the 14th Annual Meeting of ISMRM, Seattle, WA; 2006 [abstract 891].
[23] Kruger G, Glover GH. Physiological noise in oxygenation-sensitive magnetic resonance imaging. Magn Reson Med 2001;46:631–7.
[24] Maertens M, Pollman S, Hanke M, Mildner T, Moller H. Retinotopic activation in response to subjective contours in primary visual cortex. Front Hum Neurosci 2008;2(2):1–7.
[25] Schafer An, van der Zwaag W, Francis S, Head KE, Gowland PA, Bowtell RW. High resolution SE-fMRI in humans at 3 and 7 T using a motor task. Magn Reson Mater Phys 2008;21(1):113–20.
[26] Brewer AA, Liu J, Wade AR, Wandell BA. Visual field maps and stimulus selectivity in human ventral occipital cortex. Nat Neurosci 2005;8(8):1102–10.
[27] Wandell BA, Dumoulin SO, Brewer AA. Visual field maps in human cortex. Neuron 2007;56:366–84.
[28] Arcaro M, McMains S, Kastner S. Phase-encoded attention tasks reveal topographic maps in posterior parahippocampal cortex. J Vis 2008;9(6):1001a.
[29] Pruessmann KP. Parallel imaging at high field strength: synergies and joint potential. Top Magn Reson Imaging 2004;15:237–44.
[30] Van de Moortele PF, Auerbach EJ, Ugurbil K, Ritter J. Multiple area B1 shimming: an efficient, low SAR approach for T2-weighted fMRI acquired in the visual and motor cortices of the human brain at ultra-high field. Proceedings of the 17th Annual Meeting of ISMRM, Honolulu, HI; 2009 [abstract 1548].
[31] Olman CA, Moeller S, Schumacher JF, et al. Investigating the whole brain with 1.5 mm isotropic resolution and 1.5 s TRs using highly accelerated high-field fMRI. Proceedings of the 17th Annual Meeting of ISMRM, Honolulu, Hawaii; 2009 [abstract 6246].